Available online at www.sciencedirect.com
ScienceDirect
Journal of Power Sources 159 (2006) 1025–1033
JOURNAL OF POWER SOURCES
www.elsevier.com/locate/jpowsour

Transient analysis of multicomponent transport with carbon monoxide poisoning effect of a PEM fuel cell

Chien-Ping Wang, Hsin-Sen Chu *

Department of Mechanical Engineering, National Chiao Tung University, Hsinchu, Taiwan 300, ROC

Received 17 November 2005; received in revised form 6 December 2005; accepted 6 December 2005
Available online 18 January 2006

Abstract

A one-dimensional, two-phase, transient mathematical model was developed to analyze how carbon monoxide poisoning affects the performance of a PEM fuel cell. This work examines both vapor and liquid water transport inside the cell. The theoretical results indicate that a higher CO concentration results in less hydrogen coverage and a large drop in the time to reach steady state t_{ss}. The slowing of the reactions at both the anode and the cathode reduce the saturation of liquid water in the catalytic layers. The distribution of liquid water depends more strongly on the CO concentration than on dilution of hydrogen in the MEA of the fuel cell. Increasing the amount of pure hydrogen drastically increases t_{ss} for a wide range of CO contents. At a relatively low CO content, a long t_{ss} can be achieved using pure hydrogen, especially at high cell voltage, promoting the tolerance for CO and providing the desired performance of the fuel cell.

Keywords: PEM fuel cell; Two-phase; Transient evolution; CO poisoning

1. Introduction

The most efficient fuel for use in a PEM fuel cell is pure hydrogen. However, this is difficult to store and has a high cost of production. Reforming from hydrocarbons, including gasoline and alcohol is the most extensively used technique for generating hydrogen fuel for use in hydrogen proton exchange membrane fuel cells, which contain 45% hydrogen, 10 ppm CO, 15% CO_2 and 1% CH_4 [1]. CO at a concentration even as low as 5–10 ppm effectively blocks Pt reaction sites for the electro-oxidation of hydrogen [2,3]. The affinity between CO and Pt is such that even at this low concentration of CO, the consequent loss of performance is severe [4,5]. Lee et al. [4] investigated the tolerance of PtSn/C, Pt/C and PtRu/C alloy electrocatalysts for CO. Depending on the nature of the electrode material, the CO oxidation occurs at different potentials. The improvement of CO tolerance is contributed by the changes in the thermodynamics and the CO adsorption process. Murthy et al. [5] presented the steady state and transient performance of a fuel cell with relatively high concentrations of CO, for two types of gas diffusion media.

Recently, many efforts have been made to increase the tolerance of the PEM fuel cell to CO [6–11]. Schmidt et al. [6] and Divisek et al. [7] presented two methods for improving the cell performance using H_2/CO as a fuel. First, the use of Pt-Ru electrocatalysts at the anode can considerably enhance the tolerance to CO. Second, the addition of liquid hydrogen peroxide to the humidification water in the cell leads to the formation of active oxygen by the decomposition of H_2O_2. Complete recovery can be achieved for H_2 100 ppm^{-1} CO. Si et al. studied the CO tolerance of the Pt-Ru/C catalyst at elevated temperature and atmospheric pressure in a PEM fuel cell [8]. They demonstrated that the anodic polarization fell dramatically as the temperature increased, because the CO coverage was lower. Improving the activity of the catalyst with a high CO tolerance increases the rates of reaction of CO and hydrogen. Zhang et al. [9] found that CO poisoning process can be accelerated at high anode flow rate. The performance decreases substantially as the anode flow rate increases, because CO is adsorbed on the catalyst site. However, increasing the anode overpotential promotes the oxidation of CO, maintaining desired cell performance. Yu et al. [10] and Santiago et al. [11] adopted the Pt-Ru/C electrocatalyst for different electrode structures to improve the tolerance of PEMFC to CO. Water sufficiently activates the Ru surface to promote the oxidation of CO.

* Corresponding author. Tel.: +886 3 5712171x55141; fax: +886 3 5727930.
E-mail address: hschu@cc.nctu.edu.tw (H.-S. Chu).

0378-7753/$ – see front matter © 2005 Elsevier B.V. All rights reserved.
doi:10.1016/j.jpowsour.2005.12.004

Nomenclature

a	contact area of Pt catalyst ($cm^2\ cm^{-3}$)
b_{fH}	ratio of forward to backward of hydrogen adsorption (atm)
b_{fCO}	ratio of forward to backward of CO adsorption (atm)
C	concentration of reactant gas ($mol\ cm^{-3}$)
D	diffusion coefficient ($cm^2\ s^{-1}$)
i	current density ($A\ cm^{-2}$)
k	conductivity of the Nafion phase
k_{eCO}	CO electro-oxidation rate constant ($A\ cm^{-2}$)
k_{eH}	hydrogen electro-oxidation rate constant ($A\ cm^{-2}$)
k_{fCO}	CO adsorption rate constant ($A\ cm^{-2}\ atm^{-1}$)
k_{fH}	hydrogen adsorption rate constant ($A\ cm^{-2}\ atm^{-1}$)
n	number of electrons
P	total pressure (atm)
R	universal gas constant ($J\ mol^{-1}\ K^{-1}$)
s	liquid water saturation
T	temperature (K)
t	time (s)
X	molar fraction
x	distance (μm)

Greek letters

ε	porosity
ϕ	ionic potential (V)
γ	stoichiometric coefficient
θ_{CO}	coverage ratio of CO on Pt catalyst site
θ_H	coverage ratio of hydrogen on Pt catalyst site
ξ	molar area density of Pt catalyst sites ($C\ cm^{-2}$)

Superscripts

CL	catalyst layer
in	inlet at catalyst layer
M	membrane

Subscripts

CO	carbon monoxide
H_2	hydrogen
O_2	oxygen
ss	steady state
wg	vapor water
wn	liquid water in Nafion phase

In theoretical studies, Springer et al. [12] derived a mathematical model to describe CO poisoning on the catalytic sites. Chan et al. [13] combined the theoretical models developed by Springer et al. [12] and Bernardi and Verbrugge [14,15] to examine the CO kinetics. Bhatia and Wang [16] treated the characteristics of the anode catalyst layer as a boundary condition in analyzing the transient CO poisoning behaviors for various levels of CO. Baschuk and Li [17] developed a mathematical model to simulate both CO poisoning and oxygen bleeding.

Although the fuel cell performance exhibited transient variations at different CO concentrations, the actual coverage profile and the reactant gas distribution over the catalyst layer are not presented. Even the transportation of liquid water and its distribution in the MEA during transient CO poisoning are not well understood. In this work, a transient two-phase mathematical model of the poisoning effect of PEM fuel cells by CO is investigated. Various parameters are considered to promote the tolerance for CO and analyze the effect on the characteristic time t_{ss}, and thus elucidate transport phenomena inside the cell and improve its performance.

2. Theoretical model

Fig. 1 depicts the presented simulation model of the PEM fuel cell, including the anode catalyst layer, the membrane and the cathode catalyst layer. The transient two-phase theoretical CO poisoning behavior is investigated. Table 1 presents the governing equations, where gaseous hydrogen concentration C_{H_2}; the gaseous oxygen concentration C_{O_2}; the gaseous carbon monoxide concentration C_{CO}; the vapor concentration C_{wg}; the concentration of liquid water in the Nafion phase C_{wn}; the saturation of liquid water s and the ionic potential ϕ. The governing equations must be solved simultaneous for the dependent variables. The reactant gas and vapor water transport are expressed as:

$$N_i = -D_i[\varepsilon^{CL}(1-s)]^{1.5}\nabla C_i \quad (1)$$

where ε^{CL} is the total porosity and s is the liquid water saturation on both the anode and the cathode sides. The water transfer rate

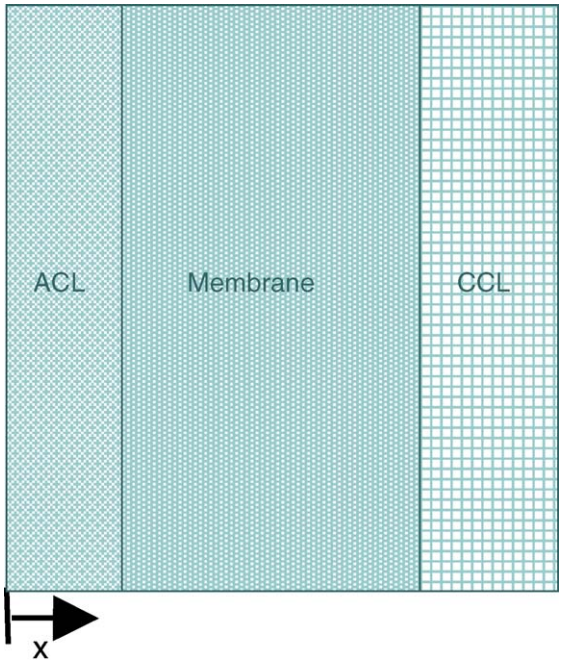

Fig. 1. A schematic model of the MEA of the PEM fuel cell.

Table 1
Governing equations

Variables	ACL	MEM	CCL
C_{H_2}	$\frac{\partial}{\partial t}[(1-s)\varepsilon^{CL}C_{H_2}] = -\nabla\cdot N_{H_2} - R_{H_2}$	$C_{H_2} = 0$	$C_{H_2} = 0$
C_{O_2}	$C_{O_2} = 0$	$C_{O_2} = 0$	$\frac{\partial}{\partial t}[(1-s)\varepsilon^{CL}C_{O_2}] = -\nabla\cdot N_{O_2} - R_{O_2}$
C_{CO}	$\frac{\partial}{\partial t}[(1-s)\varepsilon^{CL}C_{CO}] = -\nabla\cdot N_{CO} - R_{CO}$	$C_{CO} = 0$	$C_{CO} = 0$
C_{wg}	$\frac{\partial}{\partial t}[(1-s)\varepsilon^{CL}C_{wg}] = -\nabla\cdot N_{wg} - R_w$	$C_{wg} = 0$	$\frac{\partial}{\partial t}[(1-s)\varepsilon^{CL}C_{wg}] = -\nabla\cdot N_{wg} - R_w$
C_{wn}	$\nabla C_{wn} = 0$	$\varepsilon^M \frac{\partial C_{wn}}{\partial t} = D_{wn}\nabla^2 C_{wn}$	$\nabla C_{wn} = 0$
s	$\frac{\varepsilon_0^{CL}\rho_w}{M_w}\frac{\partial s}{\partial t} = \frac{\rho_w K_{w,0}}{M_w\mu_w}\left(-\frac{dP_c}{ds}\right)\left(s\nabla^2 s + (\nabla\cdot s)^2\right) + R_w$	$s = 0$	$\frac{\varepsilon_0^{CL}\rho_w}{M_w}\frac{\partial s}{\partial t} = \frac{\rho_w K_{w,0}}{M_w\mu_w}\left(-\frac{dP_c}{ds}\right)\left(s\nabla^2 s + (\nabla\cdot s)^2\right) + \left(4n_d^{CL} + 2\right)R_{O_2} + R_w$
ϕ	$k_{eff}\nabla^2\phi - (R_{H_2} + R_{CO}) = 0$	$k\nabla^2\phi = 0$	$k_{eff}\nabla^2\phi - R_{O_2} = 0$

between the gas and liquid interfacial phase used by Lin et al. [19] and He et al. [18] is used herein:

$$R_w = k_c\frac{\varepsilon_0^{CL}(1-s)y_v}{RT}(y_vP - P_v^{sat})q + k_v\frac{\varepsilon_0^{CL}s\rho_w}{M_w}(y_vP - P_v^{sat})(1-q) \quad (2)$$

The first and second term represents the condensation and evaporation rates, respectively, where q is the switching function while k_c and k_v are rate constants. The transport of liquid water in the membrane is driven by the combined effect of diffusion and electro-osmotic drag [20]:

$$N_w = -D_{wn}\frac{\partial C_{wn}}{\partial x} + \frac{i}{F}n_d \quad (3)$$

in which N_w is the flux of liquid water, D_{wn} the diffusion coefficient of liquid water, i the flux of the charges, n_d the electro-osmotic drag coefficient, and F is the Faraday constant. The transport of liquid water in the catalytic layer is described by the simplified correlation $K_w(s) = K_{w,0}s$, which elucidates the relationship between the permeability to liquid water and the saturation of liquid water [19].

In the anode catalytic layer, the distributions of the current densities of hydrogen and carbon monoxide are:

$$\frac{di_{H_2}}{dx} = 2ak_{eH}\theta_H \sinh\left(\frac{n_{H_2}F(\phi_s - \phi - U_0)}{2RT}\right) \quad (4)$$

$$\frac{di_{CO}}{dx} = 2ak_{eCO}\theta_{CO} \sinh\left(\frac{n_{CO}F(\phi_s - \phi - U_0)}{2RT}\right) \quad (5)$$

where k_{eH} and k_{eCO} are the hydrogen and CO electro-oxidation rate constants [12], ϕ_s the electronic potential, ϕ the electrolytic phase potential [21] and U_0 is the thermodynamic equilibrium potential. The coverage θ_H and θ_{CO} is [12]:

$$\xi\frac{d\theta_H}{dt} = k_{fH}X_HP(1-\theta_H-\theta_{CO}) - b_{fH}k_{fH}\theta_H - 2k_{eH}\theta_H \sinh\left(\frac{n_{H_2}F(\phi_s - \phi - U_0)}{2RT}\right) \quad (6)$$

$$\xi\frac{d\theta_{CO}}{dt} = k_{fCO}X_{CO}P(1-\theta_H-\theta_{CO}) - b_{fCO}k_{fCO}\theta_{CO} - 2k_{eCO}\theta_{CO}\exp\left(\frac{n_{CO}F(\phi_s - \phi - U_0)}{2RT}\right) \quad (7)$$

where ξ is the molar area density of the catalyst sites, X_H the molar fraction of hydrogen, X_{CO} the CO molar fraction, and P is the total pressure. The reaction rates of hydrogen and CO within the anode catalyst layer are:

$$R_{H_2} = (1-s)\frac{di_{H_2}}{dx}\left(\frac{\gamma_{H_2}}{n_{H_2}F}\right) \quad (8)$$

$$R_{CO} = (1-s)\frac{di_{CO}}{dx}\left(\frac{\gamma_{CO}}{n_{CO}F}\right) \quad (9)$$

where γ is the stoichiometric coefficient and n is the number of electrons. At the cathode catalyst layer, the reaction rate of oxygen is given by:

$$R_{O_2} = \frac{1}{4F}(1-\bar{\theta}_{CO})(1-s)ai_0 \times\left[\frac{C_{O_2}}{C_{O_2,ref}}\exp\left(\frac{-F(\phi_s - \phi - U_0)}{RT}\right)\right] \quad (10)$$

where $\bar{\theta}_{CO}$ is the mean CO coverage, which was calculated from the anodic CO coverage θ_{CO}. The factor $(1-s)$ represents the effect of liquid water saturation in the catalyst layers. The initial conditions are all steady state without zero CO. Table 2 lists all of the boundary conditions used in this simulation model. Without consideration for the gas diffusion layer, the liquid water saturation is assumed to be zero at the boundaries ($x = 0$ and L).

3. Results and discussion

Various CO concentrations and hydrogen dilutions are employed to simulate a wide range of hydrogen fuels from the reformer, and thus elucidate the transient behavior associated with poisoning. The feed vapor water is fully saturated at 80 °C at both the anode and the cathode inlets. The reactant gas distribution, the coverage, the liquid water distribution and the time to reach steady state are investigated. The initial condition is started in the absence of CO. The steady-state condition is defined as

Table 2
Boundary conditions

Variables	$x=0$	ACL/MEM	MEM/CCL	$x=L$
C_{H_2}	$C_{H_2}=C^{in}_{H_2}$	$N_{H_2}\|_{ACL}=0$	N/A	N/A
C_{O_2}	N/A	N/A	$N_{O_2}\|_{ACL}=0$	$C_{O_2}=C^{in}_{O_2}$
C_{CO}	$C_{CO}=C^{in}_{CO}$	$N_{CO}\|_{ACL}=0$	N/A	N/A
C_{wg}	$C_{wg}=C^{in}_{wg}$	$N_{wg}\|_{ACL}=0$	$N_{wg}\|_{CCL}=0$	$C_{wg}=C^{in}_{wg}$
C_{wn}	N/A	$k(C_a-C_{wn})=N_w\|_{MEM}$	$\frac{\beta i}{2F}+k(C_c-C_{wn})=-N_w\|_{MEM}$	N/A
s	$s=0$	$N_w\|_{ACL}=N_w\|_{MEM}$	$N_w\|_{MEM}=N_w\|_{CCL}$	$s=0$
ϕ	$\phi=0$	$k_{n,eff}\nabla\phi=k_n\nabla\phi$	$k_{n,eff}\nabla\phi=k_n\nabla\phi$	$\nabla\phi=0$

pertaining when the relative error of the output current density reaches 10^{-3} (A cm^{-2}):

$$\{i(n)-i(n+1)\}\le 10^{-3} \quad (11)$$

in which $i(n)$ is the current density at the nth min. Table 3 presents the parameters used in this work.

Fig. 2 plots the transient evolution of the hydrogen coverage across the anode catalyst layer with 10 ppm CO, 100% H_2 and 0.6 V. The simulation begins in the steady state without CO poisoning. Consequently, the hydrogen coverage, θ_H, decreases with time because CO is adsorbed on the Pt catalyst, reducing the number of catalytic sites available for the electro-oxidation of hydrogen. Fig. 3 shows that during poisoning CO is adsorbed on the catalytic sites, because the Pt catalyst has a strong affinity for CO. The accumulation of CO at the catalytic sites is sustained, inhibiting the electro-oxidation of hydrogen. Hence, the hydrogen and CO coverage takes 100 min to reach a steady state.

Fig. 4 shows the liquid water saturation profiles across the anode catalyst layer at different times, with 100% H_2, 10 ppm CO and 0.6 V. The effect of the electro-osmotic drag is proportional to the current density, which was generated by the electro-chemical reaction of hydrogen and oxygen. The coverage of hydrogen falls with time, so the current density was reduced, weakening the effect of electro-osmotic drag. However,

Table 3
The parameters used in the present model

Temperature, T (K)	353
Total pressure, P (atm)	1
Diffusion coefficient of hydrogen in gas phase, D_{H_2} (cm^2 s^{-1})	1.1028
Diffusion coefficient of oxygen in gas phase, D_{O_2} (cm^2 s^{-1})	$0.1775\times(T/273.15)^{1.823}$
Diffusion coefficient of vapor in gas phase, D_{wg} (cm^2 s^{-1})	$0.256\times(T/307.15)^{2.334}$
Thickness of catalyst layer, δ_{CL} (μm)	16
Thickness of membrane, δ_{MEM} (μm)	50
Gas porosity in catalyst layer, ε^{CL}	0.4
Volumetric fraction of Nafion in membrane membrane, ε_m	0.4
Ionic conductivity, k_n (mho cm^{-1})	0.17
hydrogen adsorption rate constant, k_{fH} (A cm^{-2} atm^{-1})	100
ratio of forward to backward of CO adsorption, b_{fCO} (atm)	1.7×10^{-6}

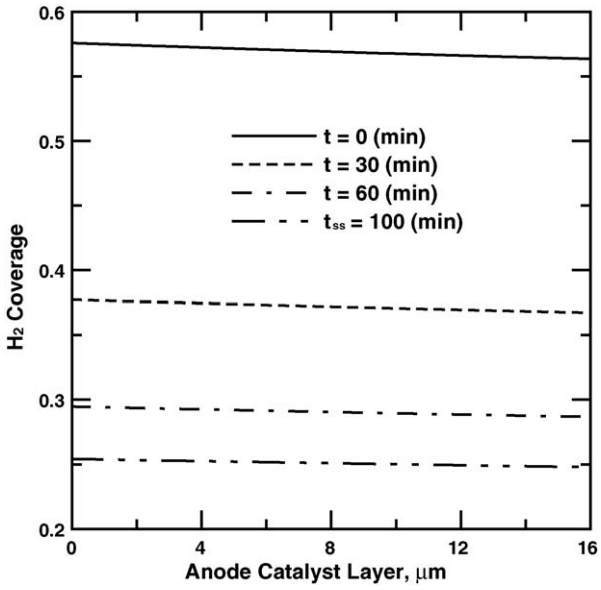

Fig. 2. The transient evolution of the hydrogen coverage profile across the anode catalyst layer, with 100% H_2, 10 ppm CO, 0.6 V.

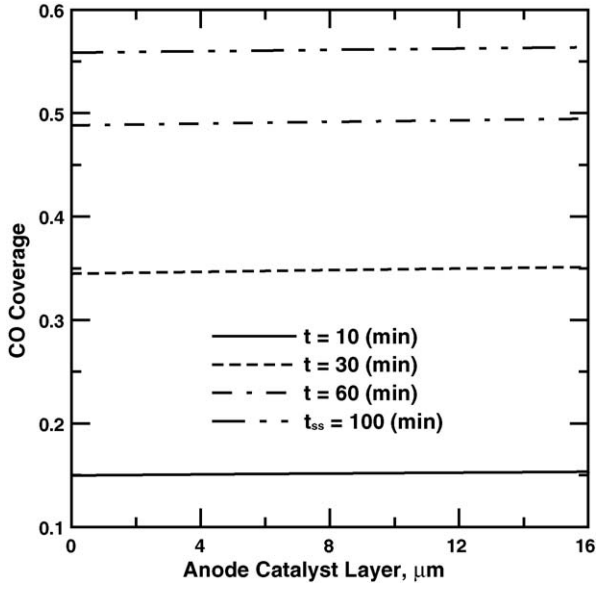

Fig. 3. The transient evolution of the CO coverage profile across the anode catalyst layer, with 100% H_2, 10 ppm CO, 0.6 V.

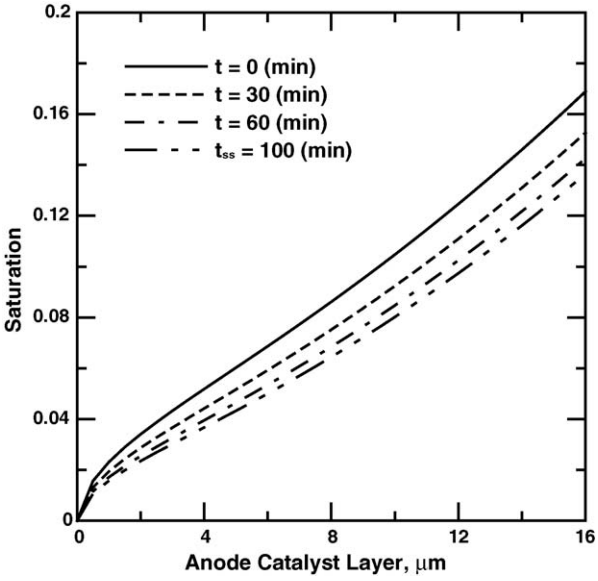

Fig. 4. The transient evolution of the liquid water saturation profile across the anode catalyst layer, with 100% H_2, 10 ppm CO, 0.6 V.

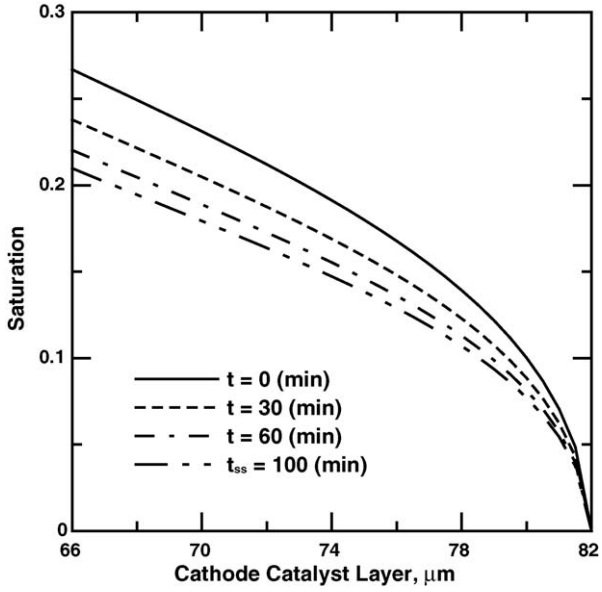

Fig. 6. The transient evolution of the liquid water saturation profile across the cathode catalyst layer, with 100% H_2, 10 ppm CO, 0.6 V.

the oxygen reduction reactions are also suppressed, reducing the diffusion of water from the cathode to the anode. Therefore, the saturation by liquid water across the anode catalyst layer decreases with time. During poisoning, the diffusion of liquid water from cathode to anode dominates the amount of liquid water at saturation in the anode catalyst layer.

Fig. 5 plots the unsteady variations of the liquid water distribution across the membrane at various times. The gradient of the liquid water distribution declines with time, because, as the duration of poisoning increases, the rate of the reaction decreases with time on both the anode and the cathode sides. The effect of electro-osmotic drag and the diffusion of liquid water from the cathode to the anode are also weakened, reducing the slope of the liquid water distribution across the membrane. Fig. 6 reveals that the amount of liquid water at saturation of the cathode catalyst layer greatly exceeds that on the anodic side of the catalyst. The small electro-osmotic drag and the generation of less liquid water cause the saturation level to drop with time.

Fig. 7 presents the ionic potential profile across the MEA at various times. No gas fuel is consumed in the membrane phase, so the ionic potential distribution plotted in Fig. 7 is a straight line. In the catalytic layers, and especially in the cathode catalyst layer, the ionic potential distribution is nonlinear, because reduction reactions consume oxygen. During poisoning, the ionic potential falls with time reducing the output current density.

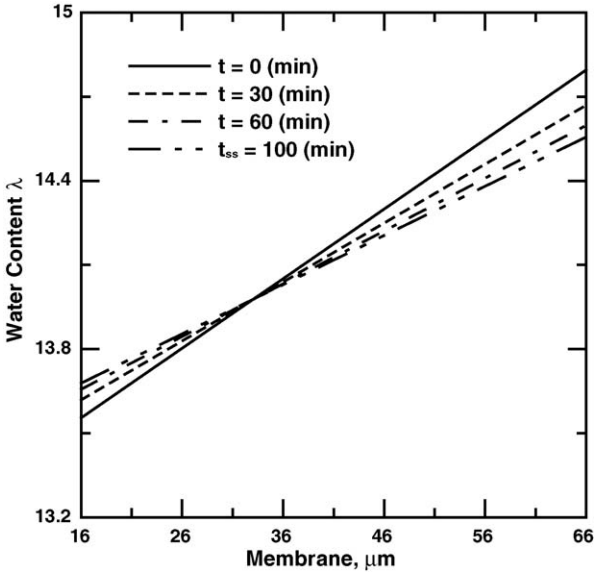

Fig. 5. The transient evolution of the water content profile across the membrane, with 100% H_2, 10 ppm CO, 0.6 V.

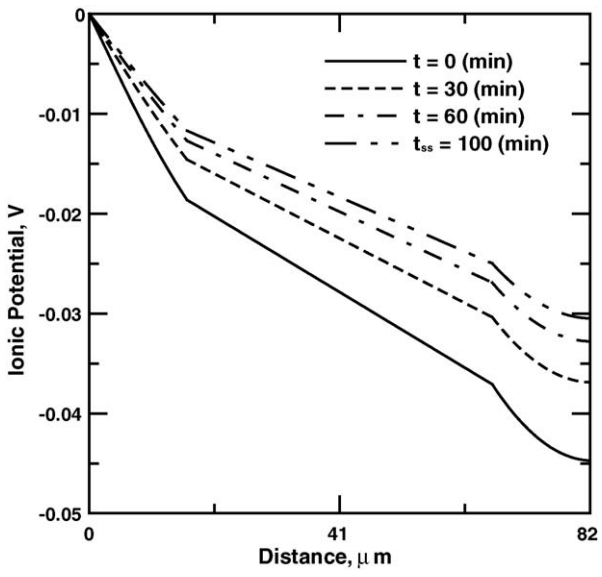

Fig. 7. The transient evolution of the ionic potential profile across the MEA, with 100% H_2, 10 ppm CO, 0.6 V.

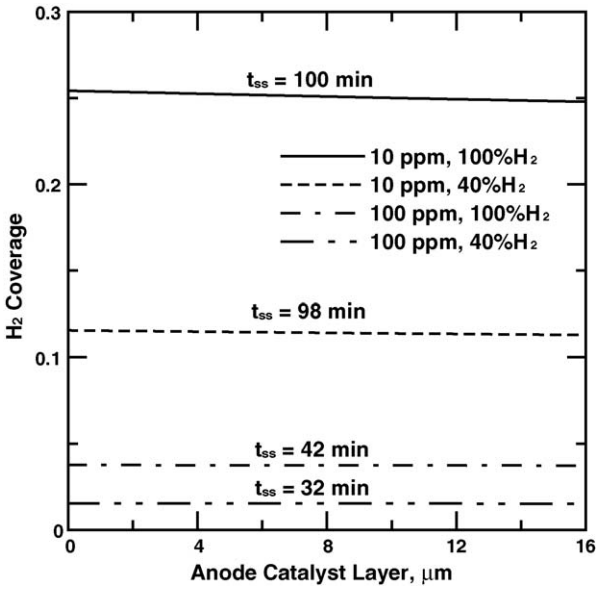

Fig. 8. The steady state hydrogen coverage profile across the anode catalyst layer at various CO concentrations and hydrogen dilutions at 0.6 V.

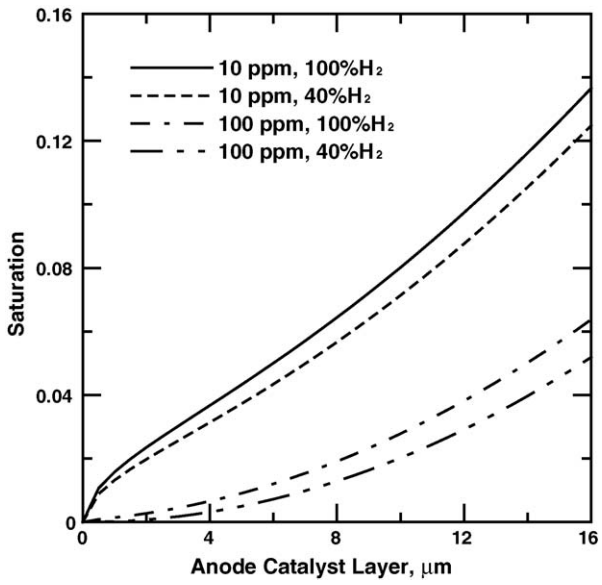

Fig. 10. The steady state liquid water saturation profile across the anode catalyst layer at various CO concentrations and hydrogen dilutions at 0.6 V.

Fig. 8 depicts the steady state hydrogen coverage profile across the anode catalyst layer at various CO concentrations and hydrogen dilutions at 0.6 V. The results indicate that at 10 ppm CO, t_{ss} is longer than at 100 ppm CO, for both 40% H_2 and 100% H_2. The hydrogen coverage is also higher at lower CO concentration, because increasing the CO concentration increases the rate of adsorption of CO onto the sites of the catalyst. Fig. 9 plots the opposite trend. Hence, hydrogen dilution significantly affects the hydrogen coverage, especially at low ppm CO. During poisoning, adding pure hydrogen fuel increase more reaction sites for hydrogen, especially at low CO concentration. As shown in Figs. 8 and 9, when an anodic inlet flow containing an H_2/CO mixture was fed into the fuel cell, CO was accumulated on the catalytic sites. The coverage of CO is much higher with 100 ppm CO, results higher total surface coverage. Nevertheless, reduces effective available catalyst sites θ_H for electro-oxidation of hydrogen.

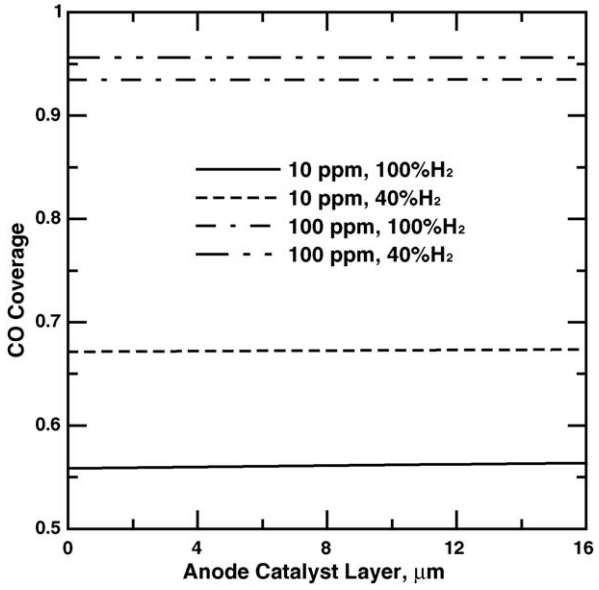

Fig. 9. The steady state CO coverage profile across the anode catalyst layer at various CO concentrations and hydrogen dilutions at 0.6 V.

Fig. 10 plots the effect of CO concentration and hydrogen dilution on the distribution of liquid water saturation across the anodic catalytic layer. Fig. 10 reveals that when cells are operated with 10 ppm CO, the amount of liquid water saturation greatly exceeds that when 100 ppm CO is used, at both 40% and 100% hydrogen. The presence of CO in the anodic inlet flow inhibits the reduction reactions on cathode side and declines the diffusion of water from the cathode to anode. The distribution of liquid water saturation depends more strongly on the CO concentration than on dilution of hydrogen in the anodic catalytic layer. Fig. 11 plots the liquid water distribution across the membrane. At 10 ppm CO, 100% H_2, the effect of the electro-osmotic drag is strong and much liquid water is generated at the cathode catalyst layer, causing the liquid water distribution to have a large slop. Consequently, the CO concentration significantly influences the distribution of liquid water across the membrane. The dilution of hydrogen by the fuel reduces the gradient of the liquid water distribution because the electro-osmotic drag is small and less water is generated in the cathode catalyst layer. An increase in the CO concentration effectively reduces the gradient of liquid water distribution across the membrane.

Fig. 12 presents the profile of liquid water saturation across the cathode catalyst layer. This figure shows that an increase in CO concentration markedly affects the liquid water saturation profile because the oxygen reduction reaction drops in the cathode catalyst layer. As the CO level increases, or the hydrogen becomes more dilute, the saturation profile becomes lower shown in Fig. 12, the CO content strongly affects the liquid saturation at the cathode catalyst layer. Fig. 13 plots the ionic potential at various CO levels and hydrogen dilutions. As discussed above, the loss of ionic potential reduces the output

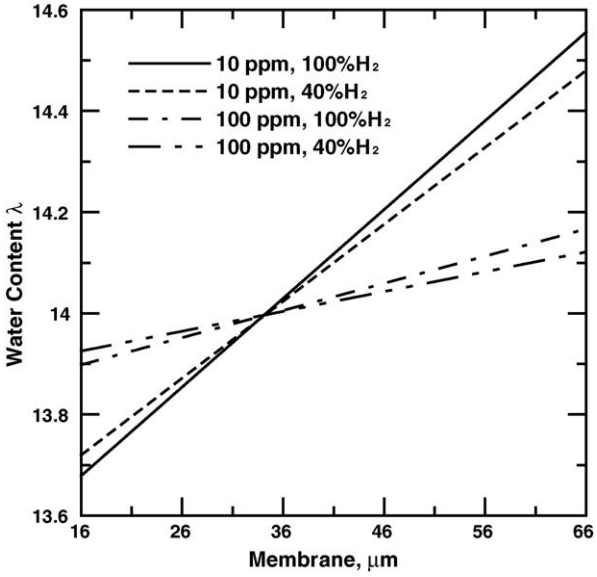

Fig. 11. The steady state water content profile across the membrane at various CO concentrations and hydrogen dilutions at 0.6 V.

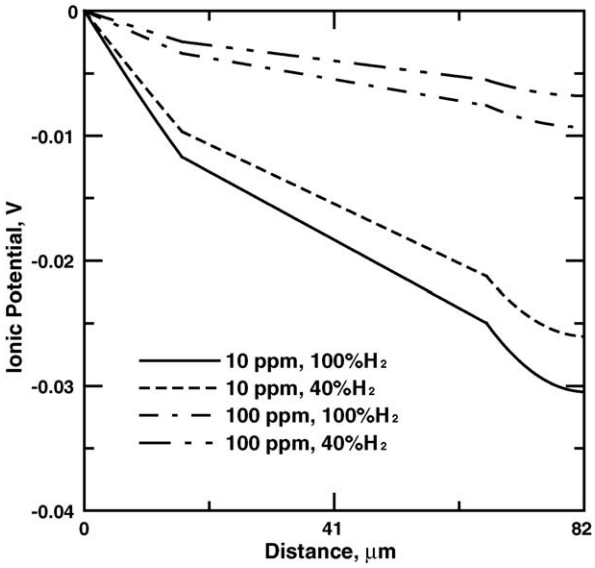

Fig. 13. The steady state ionic potential profile across the MEA at various CO concentrations and hydrogen dilutions at 0.6 V.

current density. Therefore, increasing the CO level or diluting the hydrogen seriously reduces the loss of ionic potential.

Fig. 14 compares the presented simulation results with experimental data reported by Bhatia and Wang [16]. There are four gas compositions fed into the anode. The simulation results show that the cell performance and durability depends strongly on the dilution of hydrogen and CO concentration, considerably reducing the current density and the time t_{ss} required to reach a steady state. Increasing hydrogen dilution and CO concentration degrades the performance of the cell and reduces the time t_{ss}. At a low level of CO (10 ppm CO), the cell performance depends more strongly on the dilution of hydrogen, considerably reducing the current density. The predicted CO poisoning results agree closely with the experimental values, except from the case for 10 ppm, 40% H_2. The discrepancy may be attributed without consideration for the gas diffusion layer. The assumption may probably influence the distribution of liquid water in the catalyst layers. This may explain the discrepancy between the predicted simulation results and experiments.

Fig. 15 plots the influence of CO concentration on the time to reach the steady state for two hydrogen dilutions and cell voltages. The theoretical results indicate that a higher CO concentration results in large drop in the time to reach steady state t_{ss}. The dropping rate of t_{ss} becomes small at a large CO content. Hydrogen dilution substantially increases time t_{ss} under a wide range of CO content. At high cell voltages, a large time t_{ss} is obtained, especially at small CO content, because only a small amount of hydrogen is used at low current density, so its

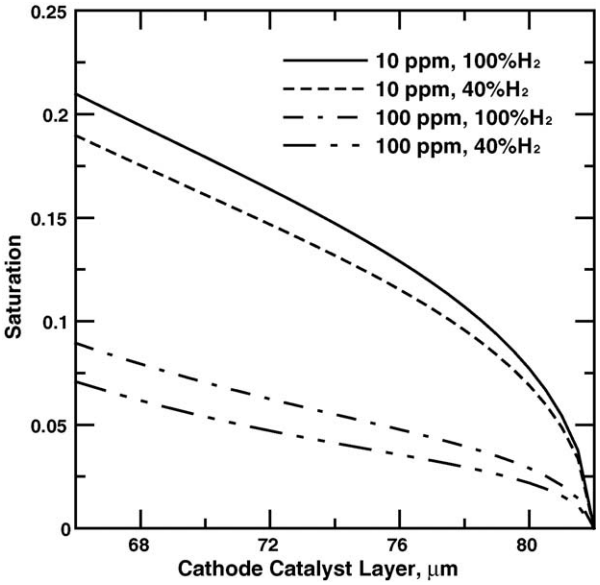

Fig. 12. The steady state liquid water saturation profile across the cathode catalyst layer at various CO concentrations and hydrogen dilutions at 0.6 V.

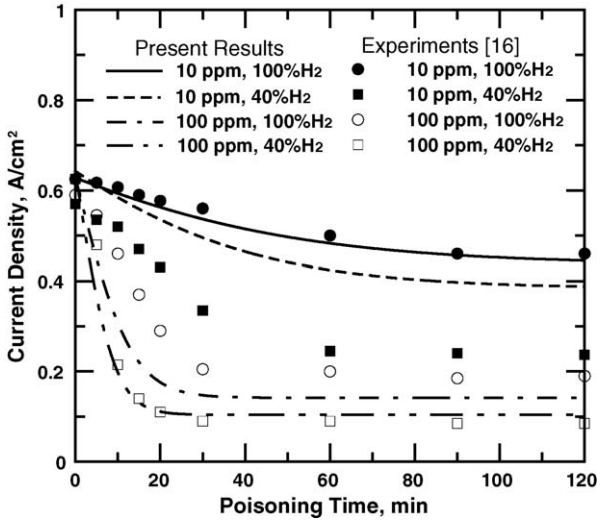

Fig. 14. The present simulation results compared with experimental data at 0.6 V.

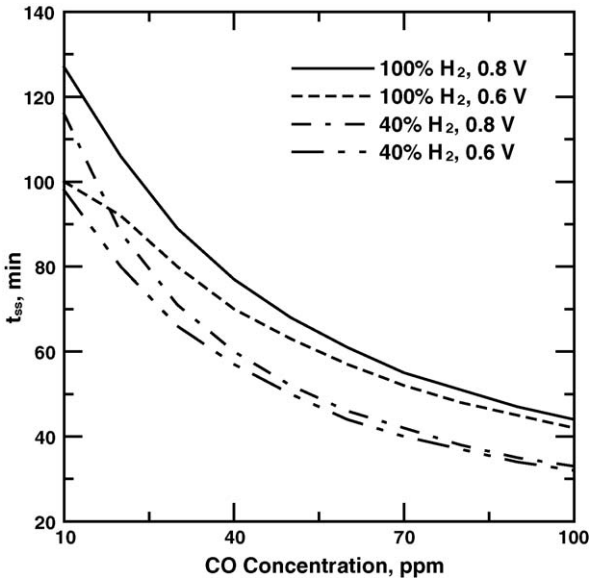

Fig. 15. The influence of CO concentration on the time to reach steady state for two hydrogen dilutions and cell voltages.

effect on the CO adsorption rate in the anode catalyst layer is weak. However, the cell voltage only weakly influences the time t_{ss} at high CO content. In this study, increasing the amount of pure hydrogen drastically increases t_{ss} for a wide range of CO contents.

The results for pure and 40% hydrogen at two CO contents are plotted for comparison in Fig. 16. A higher CO content corresponds to lower t_{ss}. At 100 ppm CO, the cell voltage does not clearly affect t_{ss}. A large time t_{ss} can be achieved using pure hydrogen. At 10 ppm CO, a small difference on t_{ss} is observed at low cell voltage for pure and 40% hydrogen. Thereafter, the time t_{ss} increases markedly as the cell voltage increases for pure and 40% hydrogen at 10 ppm CO. Fig. 16 reveals that a long

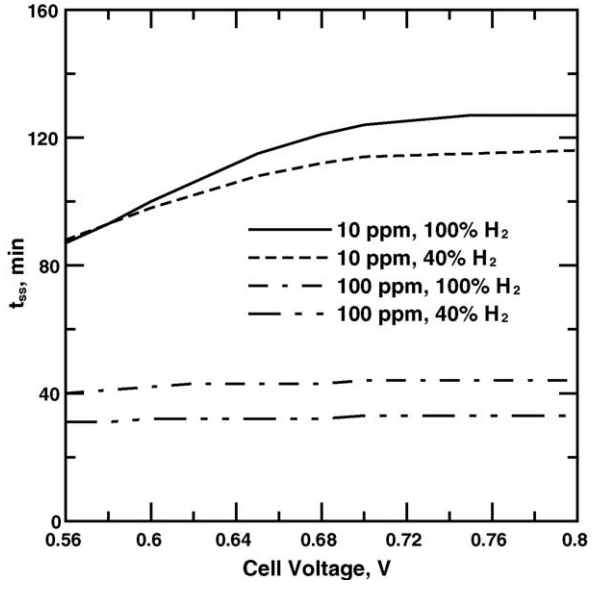

Fig. 16. The effect of cell voltage on the time to reach steady state for two hydrogen dilutions and CO concentrations.

t_{ss} can be achieved containing pure hydrogen at 10 ppm CO, especially at high cell voltage.

4. Conclusions

This study investigated the transient nature of poisoning from carbon monoxide across the MEA of the PEMFC is investigated. Hydrogen dilution and CO content drastically affect the performance and durability of the fuel cell. When an anodic inlet flow containing an H_2/CO mixture was fed into the fuel cell, CO is accumulated on the catalytic sites. This is because the Pt catalyst has a strong affinity for CO, inhibiting the electro-oxidation of hydrogen. The hydrogen coverage and liquid water saturation declines as the reaction proceeded. The gradient of the liquid water distribution across the membrane and the ionic potential also fell with time. The distribution of liquid water depends more strongly on the CO concentration than on dilution of hydrogen in the MEA of the fuel cell. The theoretical results indicate that a higher CO concentration results in large drop in the time to reach steady state t_{ss}. In this study, increasing the amount of pure hydrogen drastically increases t_{ss} for a wide range of CO contents. At 100 ppm CO, the cell voltage does not clearly affect t_{ss}. A large time t_{ss} can be achieved using pure hydrogen. At low CO content, the influence of hydrogen dilution on the time t_{ss} is weak at low cell voltage. Thereafter, the time t_{ss} increases markedly as the cell voltage increases at low CO content. When the anode inlet flow contains pure hydrogen, a long t_{ss} results, especially at low ppm of CO and high cell voltage, providing the desired performance and durability of the fuel cell.

Acknowledgements

The authors highly appreciate Professor Falin Chen, Chyi-Yeou Soong and Wei-Mon Yan for their help. This study was supported by the National Science Council, the Republic of China, through the grant NSC 93-2212-E-009-001.

References

[1] R.C. Urian, A.F. Gulla, S. Mukerjee, J. Electroanal. Chem. 554–555 (2003) 307–324.
[2] J. Zhang, R. Datta, J. Electrochem. Soc. 149 (2002) A1423–A1431.
[3] B.N. Grgur, N.M. Markovic, P.N. Ross, J. Electrochem. Soc. 146 (1999) 1613–1619.
[4] S.J. Lee, S. Mukerjee, E.A. Ticianclli, J. McBreen, Electrochim. Acta 44 (1999) 3283–3293.
[5] M. Murthy, M. Esayian, A. Hobson, S. Mackenzie, W. Lee, J.W. Van Zee, J. Electrochem. Soc. 148 (2001) A1141–A1147.
[6] V.M. Schmidt, H.-F. Oetjen, J. Divisek, J. Electrochem. Soc. 144 (1997) L237–L238.
[7] J. Divisek, H.-F. Oetjen, V. Peinecke, V.M. Schmidt, U. Stimming, Electrochim. Acta 43 (1998) 3811–3815.
[8] Y. Si, R. Jiang, J.C. Lin, H.R. Kunz, J.M. Fenton, J. Electrochem. Soc. 151 (2004) A1820–A1824.
[9] J. Zhang, T. Thampan, R. Datta, J. Electrochem. Soc. 149 (2002) A765–A772.
[10] H. Yu, Z. Hou, B. Yi, Z. Lin, J. Power Sources 105 (2002) 52–57.
[11] E.I. Santiago, V.A. Paganin, M. do Carmo, E.R. Gonzalez, E.A. Ticianelli, J. Electroanal. Chem. 575 (2005) 53–60.

[12] T.E. Springer, T. Rockward, T.A. Zawodzinski, S. Gottesfeld, J. Electrochem. Soc. 148 (2001) A11–A23.
[13] S.H. Chan, S.K. Goh, S.P. Jiang, Electrochim. Acta 48 (2003) 1905–1919.
[14] D.M. Bernardi, M.W. Verbrugge, J. Electrochem. Soc. 37 (1991) 1151–1163.
[15] D.M. Bernardi, M.W. Verbrugge, J. Electrochem. Soc. 139 (1992) 2477–2491.
[16] K.K. Bhatia, C.Y. Wang, Electrochim. Acta 49 (2004) 2333–2341.
[17] J.J. Baschuk, X. Li, Int. J. Energy Res. 25 (2003) 1095–1116.
[18] W. He, J.S. Yi, T.V. Nguyen, AICHE J. 46 (2000) 2053–2064.
[19] G. Lin, W. He, T.V. Nguyen, J. Electrochem. Soc. 151 (2004) A1999–A2006.
[20] T. Okada, G. Xie, Y. Tanabe, J. Electroanal. Chem. 413 (1996) 49–65.
[21] Y. Wang, C.Y. Wang, Electrochim. Acta 50 (2005) 1307–1315.